Article

Redox metabolism measurement in mammalian cells and tissues by LC-MS

Boryana Petrova [1,2], **Anna Warren** [1,†], **Nuria Yulia Vital** [1,†], **Adam G. Maynard** [1,3], **Alan Wong** [1,3,4] **and Naama Kanarek** [1,2,5]*

[1] Department of Pathology, Boston Children's Hospital, 300 Longwood Avenue, Boston, MA 02115, USA
[2] Harvard Medical School, Boston, MA 02115, USA
[3] Program in Biological and Biomedical Sciences, Harvard Medical School, Boston, MA 02115, USA
[4] Harvard/MIT MD-PhD Program, Harvard Medical School, Boston, MA 02115
[5] Broad Institute of Harvard and Massachusetts Institute of Technology, 415 Main Street, Cambridge, MA 02142, USA.
† These authors contributed equally to this work.
* Correspondence: naama.kanarek@childrens.harvard.edu; Tel.: +1-617-919-7352

Abstract: Cellular redox state is highly dynamic and delicately balanced between constant production of reactive oxygen species (ROS), and neutralization by endogenous antioxidants, such as glutathione. Physiologic ROS levels can function as signal transduction messengers, while high levels of ROS can react with and damage various molecules eliciting cellular toxicity. The redox state is reflective of the cell's metabolic status and can inform on regulated cell-state transitions or various pathologies including aging and cancer. Therefore, methods that enable reliable, quantitative readout of the cellular redox state are imperative for scientists from multiple fields. Liquid-chromatography mass-spectrometry (LC-MS) based methods to detect small molecules that reflect the redox balance in the cell such as glutathione, NADH and NADPH, have been developed and applied successfully, but because redox metabolites are very labile, these methods are not easily standardized or consolidated. Here we report a robust LC-MS method for the simultaneous detection of several redox-reactive metabolites that is compatible with parallel global metabolic profiling in mammalian cells. We performed a comprehensive comparison between three commercial hydrophilic interaction chromatography (HILIC) columns, and we describe the application of our method in mammalian cells and tissues. The presented method is easily applicable and will enable the study of ROS function and oxidative stress in mammalian cells by researchers from various fields.

Keywords: redox metabolites; mass-spectrometry method; HILIC chromatography; NADH; NADPH; Glutathione; redox metabolite detection in mammalian cells

1. Introduction

Cellular redox could be defined as the highly dynamic and tightly regulated balance between molecules that function as oxidants and antioxidants. Cells constantly produce reactive oxygen species (ROS) through partial reduction of O_2 by the electron transport chain (ETC). ROS are inactivated by enzymes such as catalase, and endogenous metabolites that function as antioxidants, such as glutathione. ROS have a role in signal transduction [1] and are therefore important for normal physiology [2]. However, if ROS levels exceed their tightly-controlled normal levels, they induce oxidative stress, and can cause damage to proteins, lipids and DNA [3]. Thus, redox state must be finely tuned to match the specific metabolic need of the cell or tissue.

The various roles played by ROS in physiological and pathological conditions draw the attention of researchers from diverse biological fields, including cancer [4, 5], immunology [6, 7], neurobiology [8], aging [9], and more. To study ROS, either in the context of ROS as signaling molecules, or as a

cause for oxidative stress, it is imperative to be able to experimentally measure cellular ROS levels, and to portray the cellular redox state. Measuring ROS is a long-standing challenge [10-12], and is still an active area of investigation. Measurement of ROS should be carefully done as each marker can be very cell-specific and biological variability could be significant among different conditions and biological systems [11]. Approaches can be broadly divided into three categories: measuring ROS directly, measuring the oxidative damage that results from high ROS, or assessing the metabolic redox state by determining reduced and oxidized redox-reactive small molecule pools. For direct measurement of ROS, several probe-assisted methods have been developed recently that measure a distinct ROS species by either a genetically encoded sensor or by positron emission tomography (PET) probe tracing [13-20].

However, for many researchers, the global cellular redox state is the more relevant readout of oxidative balance because it is the sum of oxidizing and reducing potential that dictates cell fitness and functionality [5]. Cellular redox state can be assessed by profiling the ratio of reduced and oxidized redox-reactive small molecules such as reduced- to oxidized-glutathione (GSH/GSSG), nicotinamide adenine dinucleotide (NAD) to reduced NAD (NAD/NADH), and nicotinamide adenine dinucleotide phosphate (NADP) to reduced NADP (NADP/NADPH). These small molecules are directly accessible by liquid-chromatography coupled to mass-spectrometry (LC-MS). Indeed, LC-MS based detection of these metabolites has been successfully applied in mammalian cells and organisms and revealed very impactful new biology in various fields [21-24]. However, by nature, redox-reactive metabolites are very labile, therefore, their extraction and detection are challenging, and results can be misleading. Furthermore, improvement of direct LC-MS quantitation has lagged, and especially missing is an integrated protocol for measurement of redox-reactive metabolites in parallel to other polar metabolites, that are often of interest for the study. Therefore, we recognized a need for a robust protocol for consistent detection of redox-reactive metabolites that can be done in parallel to global metabolite detection methods in mammalian cells. This can provide information about the general metabolic state of the cell side by side with its redox state.

Here we describe a LC-MS method for detection of redox-reactive metabolites (hereafter; redox metabolites) in parallel to global metabolic profiling in mammalian cells. We have performed a comprehensive comparison between three commercially available chromatography columns; Accucore Amide HILIC (Thermo-Fisher Scientific), LUNA-NH2 (Phenomenex) or SeQuant ZIC-pHILIC (Millipore-Sigma), and optimized extraction method for mammalian cells, tissues, and physiological fluids. Our protocol and data provide guidance for optimization of the LC-MS method to allow for tailored metabolite profiling of redox metabolites in parallel to other metabolites of interest.

2. Results

2.1. A method to quantify redox metabolites by LC-MS

To address the need for quantification of redox metabolites in parallel to detection of polar metabolites from mammalian cells we set to optimize an LC-MS method based on hydrophilic interaction chromatography (HILIC). In addition to the well recognized SeQuant ZIC-pHILIC columns (Millipore-Sigma) we decided to explore two more consistently aviailable columns: Accucore-Amide HILIC (Thermo-Fisher Scientific) and LUNA-NH2 (Phenomenex). We first optimized chromatographic solvents, gradient and temperature based on literatute [25, 26] and aiming for a broad metabolite coverage (generally in the basic pH range). When comparing the chromatography and detection of several common intracellular metabolites such as amino acids, nucleotides, lactate, and glucose, we observed variation in ionization efficiency of these metabolites, as well as varying peak widths and retention times (Figure 1a and Table 1). However, because most metabolites were well detected via all three columns, we decided to use all three for optimization of the redox metabolites detection method. We focused our efforts on NAD+, NADH, NADP, NADPH, GSH and GSSG, as these metabolites are critical for redox balance and are most commonly assessed as a readout for the cellular redox state. As NAD+ and NADP are in the same molecular weight range as well as significanlty more stable than their reduced counterparts, we excluded them from our

initial optimization of mass spectrometry parameters (Figure 1b, c). Conversely, we assessed optimization parameters and the detection efficiency of both native GSH and GSH derivatized with Ellman's reagent (5,5'-dithiobis-2-nitrobenzoic acid) [27] (abbreviated GSH-Ell; Figure S1a and b). We were capable to reliably and reproducibly detect all tested redox metabolite standards on all three HILIC columns, although sensitivity varied among the columns (Figure 1b). We operate a Thermo QE mass spectrometer under heated electrospray ionization (HESI) conditions. To optimize detection by MS of the redox metabolite standards we tested various HESI source parameters (Figure 1c and Figure S1c), and compared the limit of detection and linearity (Figure 1d). We observed linear detection for almost all redox metabolites in all three columns with the exception GSH-Ell on the LUNA-NH2 column. Notably, compared to GSH and other small molecular weight standards (Figure S1c), GSH-Ell has HESI parameters closer to NAD(P)H and GSSG while at the same time a limit of detection similar to GSH on ZIC-HILIC and Accucore columns, offering the possibility to combine optimum parameters for the detection of all relevant redox reactive pairs. In summary, following method optimization, all three columns tested here are suitable for detection of NADH, NADPH, GSH and GSSG and our protocols can be applied directly by laboratories that work with any of these chromatography columns.

Table 1. Retention times and HESI polarity mode for metabolite standards shown in Figure 1. Three chromatographic column separations are indicated. Further details can be found in Table S1.

Standard name	Exact mass	neg m/z	pos m/z	mode	RT (min.) ZIC-pHILIC	RT (min.) Accucore HILIC	RT (min.) LUNA-NH2
Alanine	89.0477	88.0404	90.055	pos	8.85	10.4	8.1
ATP	506.9958	505.9885	508.003	neg	10.83	9.96	15.75
Citric acid	192.027	191.0197	193.0343	neg	12.23	9.7	13.42
Glucose	180.0634	179.0561	181.0707	neg	9.33	7.5	6.46
Glutamine	146.0691	145.0619	147.0764	pos	9.13	9.12	8.92
Histidine	155.0695	154.0622	156.0768	pos	9.31	12	9.47
Inosine	268.0808	267.0735	269.088	pos	5.98	4.3	8.69
Lactic acid	90.0317	89.0244	91.039	neg	5.41	2.82	6.46
Malic acid	134.0215	133.0142	135.0288	neg	10.74	6.6	11.56
Choline phosphate	183.066	182.0588	184.0733	pos	10.17	14.66	10.95
Proline	115.0633	114.0561	116.0706	pos	7.22	9.04	7.67
Pyruvic acid	88.016	87.0084	89.0233	neg	4.32	2.34	N/A
Tryptophan	204.0899	203.0826	205.0972	pos	6.25	4.08	7.61
Tyrosine	181.0739	180.0666	182.0812	pos	6.16	5.85	8.71
Uracil	112.0273	111.02	113.0346	neg	4.1	3.67	3.66
Uridine	244.0695	243.0623	245.0768	neg	4.81	5.38	5.13
Glutathione	307.0838	306.0765	308.0911	pos	9.64	12.80	11.13
Oxidized glutathione	612.1520	611.1447	613.1592	pos	11.95	15.02	13.55
GSH-Ellman's	504.0625	503.0552	505.0698	neg	9.85	12.07	12.02
NAD+	664.1170	662.1019	664.1164	pos	9.36	12.69	10.99
NADH	665.1248	664.1175	666.1320	pos	8.85	12.22	12.60
NADP+	744.0833	742.0682	744.0827	pos	11.13	14.95	14
NADPH	745.0911	744.0838	746.0984	pos	11.44	14.15	16.24

2.2. Optimization of redox metabolite detection in mammalian cells

Following the reliable and sensitive detection of redox metabolites by LC-MS, we set out to optimize extraction solvent and storage conditions for detection of the endogenous metabolites in mammalian cells. We tested three extraction buffers for optimal metabolite extraction from the mammalian cell line K562. The buffers A, B, and C (Table 2) were used in an identical extraction protocol and analyzed using the ZIC-pHILIC column for LC-MS.

Table 2. Extraction buffer composition.

Buffer	Composition	Reference
A	40:40:20 acetonitrile:methanol:water, 0.1M formic acid	[28] Lu W, et al. Antioxid Redox Signal. 2018 Jan 20;28(3):167-179.
B	80% methanol, 20% 25 mM Ammonium Acetate, 2.5 mM Na-Ascorbate	[29] Chen L, et al. Anal Bioanal Chem. 2017 Oct;409(25):5955-5964.
C	Solution1: 100% Methanol Solution2: 25mM Ammonium Acetate, 2.5mM Na-Ascorbate Use 80% Solution 1/20% Solution 2	
C + Ellman's	20mM Ellman's in Solution 2	[27] Ellman, G.L., *Tissue sulfhydryl groups.* Arch Biochem Biophys, 1959. **82**(1): p. 70-7

We used three increasing amounts of cells to demonstrate the reproducibility and linearity of the results (Table 3).

Table 3. Linearity and reproducibility for four buffer comparisons. R squared (R^2) values were calculated based on linearity of fit between relative change and cell count. Coefficient of variation (CV) was calculated considering the variability between two biological replicates for three cell counts.

Buffer	R^2		CV (%)	
A	GSH	0.9999	GSH	5.36
	GSSG	0.9999	GSSG	8.76
	NAD+	0.9999	NAD+	3.52
	NADP	0.9970	NADP	5.72
	NADPH	0.8614	NADPH	28.18
B	GSH	0.9999	GSH	5.96
	GSSG	0.9988	GSSG	56.18
	NAD+	0.9999	NAD+	7.43
	NADP	0.7124	NADP	78.45
	NADPH	N/A	NADPH	N/A
C	GSH	0.9254	GSH	25.98
	GSSG	0.9828	GSSG	17.93
	NAD+	0.9996	NAD+	3.75
	NADP	0.9986	NADP	5.93
	NADPH	0.7407	NADPH	63.25

	GSH	0.9983		GSH	3.44
	GSSG	0.9973		GSSG	23.60
C + Ellman's	NAD+	0.9999		NAD+	5.57
	NADP	0.9984		NADP	3.85
	NADPH	0.9999		NADPH	11.16

Buffer A appeared sub-optimal for detection of NADPH, while buffer B was suboptimal for NADPH and NADP detection (Figure 2a). Buffer C was suitable for detection of GSH, NADH, NAD+ and NADP, but not NADPH. Of note are the lower levels of GSSG in Buffer C and C+Ell; oxidation of GSH to GSSG and GSSG extraction efficiency are confounding factors when it comes to the total measured GSSG levels, however, the presence of ascorbate in the buffer (as in buffers B and C) as well as Ellman's reagent (as in buffer C+Ell) likely prevent oxidation of GSH and thus lead to lower levels of detected GSSG. Further, the addition of the Ellman's reagent to buffer C resulted in reproducible detection of GSH-Ell as well as of NADPH, likely as a result of the stabilization of GSH and its indirect effect on stabilizing NADPH levels [30] (Figure 2a). All buffers were suitable for detection of other metabolites such as amino acids (Figure S2a). We further tested the stability of endogenous redox metabolites in mammalian cell extracts using extraction buffers B and C at various storage conditions (Figure 2b). We observed no significant decline in signal with storage at -80 °C and the additional storage at 4°C (4 or 24 hours) for amino acids (Figure S2b) and for the redox metabolites we measured, with the exception of a small decline of GSH, NADH and NADPH in buffer B and of NADH in buffer C and C+Ell after 24h at 4°C (Figure 2c).. In summary, buffer C+Ell showed optimal in terms of storage stability and linerity of endogenous redox metabolites detection in K562 cells.

2.3. Application of the redox metabolite detection method for mammalian tissues

Next, we applied our method for detection of redox metabolites in parallel to global metabolic profiling of mammalian tissues. We focused on mouse liver and kidney, because we wanted to test our method in organs with high metabolic complexity. We compared the detection of 215 polar metabolites by the three HILIC columns; Accucore Amide HILIC, LUNA-NH2, and ZIC-pHILIC in mouse liver (Figure 3a and S3a), and kidney (Figure 3b and S3b). We observed significant differences between these columns, with specific metabolites detected better in each column, where ZIC-pHILIC had the broadest coverage (Table 4 and Figure S3a and S3b). The reported results here can guide researchers in selecting preferred column based on specific metabolites of interest.

Table 4. Linearity and reproducibility for three HILIC columns. R squared (R^2) values per metabolite were calculated based on linearity of fit between measured relative change in pooled samples and corresponding dilution factor. Coefficient of variation (CV) per metabolite was calculated from re-injections of pooled samples. Indicated are number of metabolites which pass indicated thresholds.

Column	Metabolites - R^2	Metabolites - CV (%)
ZIC	121 - 0.97	152 - 30%
	122 - 0.95	141 - 20%
Acc	69 - 0.97	78 - 30%
	69 - 0.95	58 - 20%
LUNA	26 – 0.97	79 - 30%
	39 - 0.95	45 - 20%

We also compared the detection of polar metabolites following extraction of mouse liver using three extraction buffers; B, C, C plus Ellman's (Table S2). We observed no significant difference between these extraction buffers overall (Figure S3c), with the exception of few specific metabolites that were detected better in each buffer (Figure 3c and 3d). Redox metabolites; GSH, GSSG, NAD, NADH, , and

NADP were well detected in mouse liver and kidney, while NADPH was well detected in liver only. Additionally, oxidized and reduced glutathione were detected in mouse cerebrospinal fluid (CSF) extracted in buffer C and in buffer C+Ell (Figure 3e). Other metabolites, such as amino acids, were well-detected in all three buffers (Figure S3d). The detection of GSH in the CSF was more consistent and reliable when the sample was extracted in buffer C plus Ellman's reagent, likely due to high oxidation rate of metabolites in the CSF. We found that liver GSH is optimally derivatized with as little as 20 μmol Ellman's reagent (Figure S3e). Sample drying and reconstitution can help concentrate low abundance metabolites when small amounts are analysed. However, given the high abundance of metabolites in liver samples, we asked if we could omit these steps prior to LC-MS analysis. This could have the added advantage of speeding up the preparation time and minimizing exposure to oxigen. In mouse liver samples, detection of NADH and NADPH was indeed improved when we did not apply drying of the sample (Figure S3f). We conclude from these results that our LC-MS method is adequate for the detection of redox metabolites in parallel to global metabolic profiling of mammalian tissues. When feasible, skiping the drying step and derivatizing GSH with Ellmans reagent can lead to better detection of redox metabolites while not compromising the vast majority of other polar metabolites.

2.4 Application of the redox metabolite detection method for profiling redox state following pharmacologic perturbations of redox balance in cells

We wanted to test our redox metabolite detection method in mammalian cells following perturbation of the redox state. To that end, we treated cells with either the reactive oxygen species H_2O_2, the oxidizing agent, diamide (DA)[31], or with oligomycin (OM) - an inhibitor of ATP synthase [32] that inhibits the electron trasport chain (ETC), and causes accumulation of NADH. We also monitored cellular redox balance following treatment with the drug methotrexate, which was shown to cause oxidative damage in mammalian tissues [33-35] and that is commonly used as a chemotherapeutic agent for the treatment of blood cancers [36]. Importantly, our method allowed us to profile, in parallel, the cell's global metabolome in response to the treatments (Figure 4a and Figure S4a, b and c) and to verify that the applied treatments resulted in the predicted changes in the metabolic profile of the cells (Figure S4c). As expected, H_2O_2, DA, and OM treatments resulted in a decreased GSH/GSSG ratio due to the oxidative conditions they induce in the cells, treatement with the oxidizing agents H_2O_2 and DA resulted in decreased NADH, and ETC inhibition by OM resulted in accumulation of NADH. NADPH levels increased following all treatments, indicating the anti-oxidative response of the cells to all treatments [37, 38] (Figure 4b). These results emphasize our ability to detect the high adaptability of the cancer cells we tested and their dynamic response to oxidative stress.

2.2. Figures, Tables and Schemes
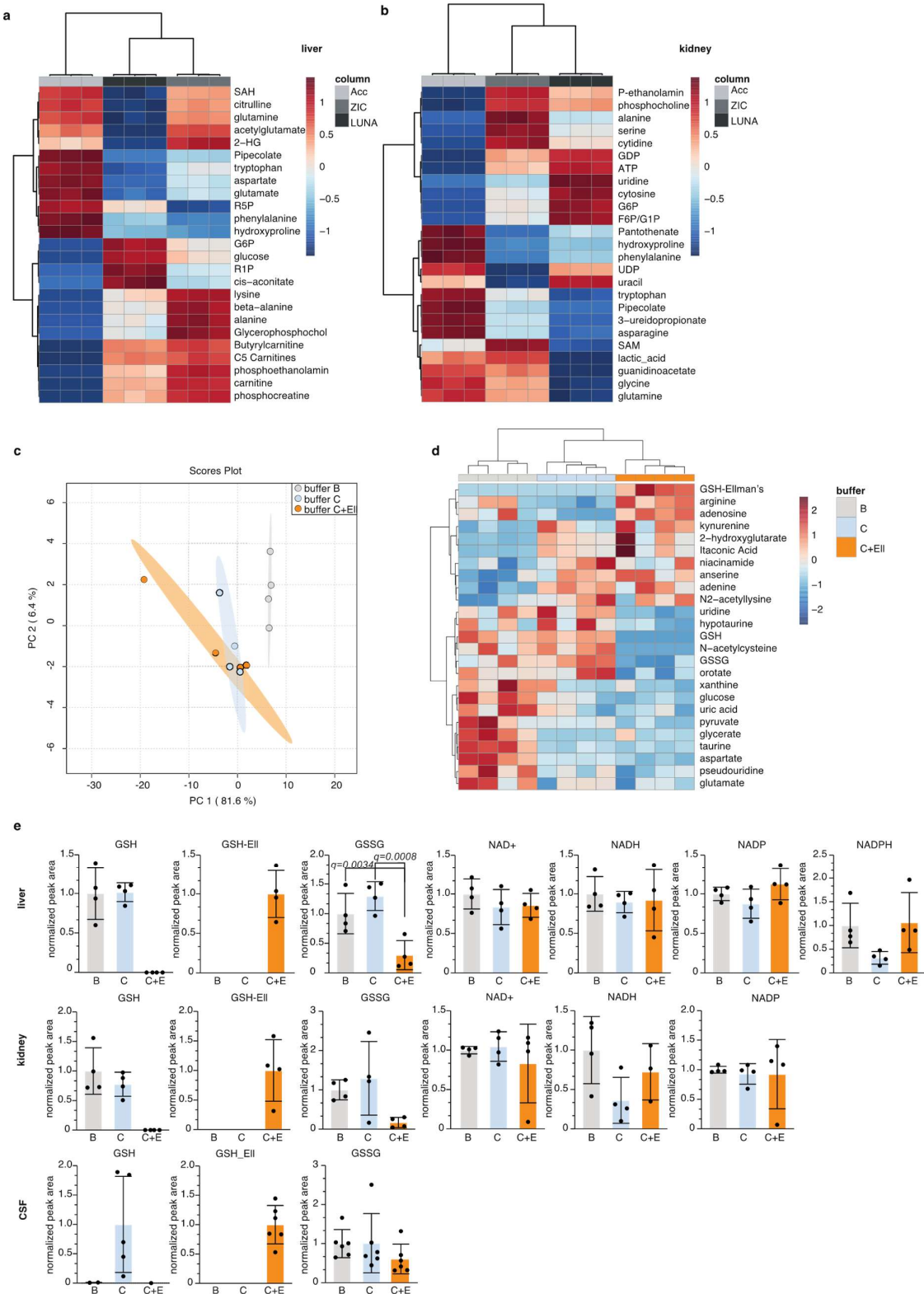
FIGURE 1
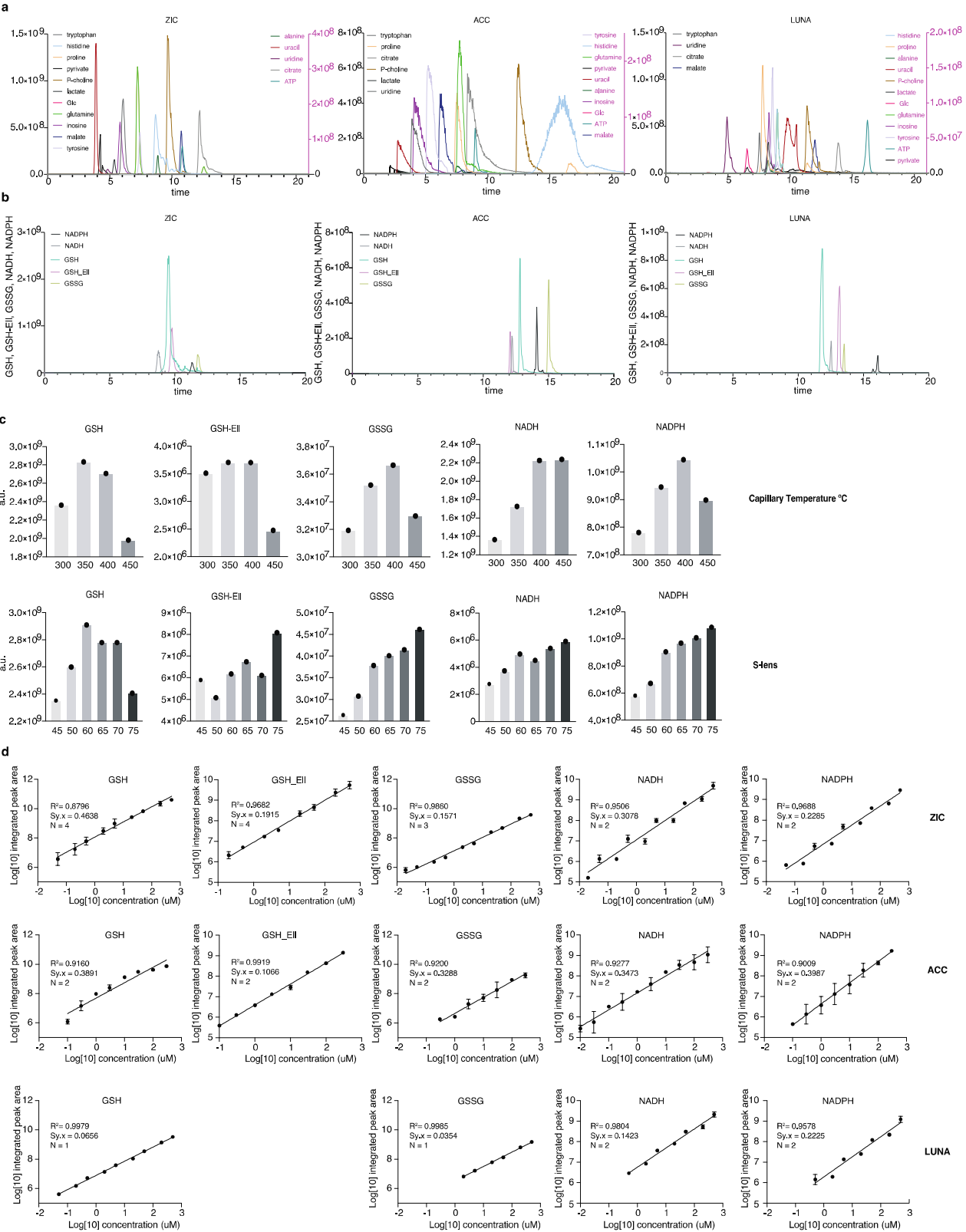
Figure 1. A method to quantify redox metabolites by LC-MS; (**a and b**) Retention times and sensitivity comparison between three HILIC-based chromatography methods. Chromatographic runs were carried out on either ZIC-pHILIC (ZIC), Accucore-NH2 (ACC), or LUNA-NH2 (LUNA). Overlaid peaks are shown for the indicated range of (a) polar metabolites (see Table S1 for further details) and (**b**) NADPH, NADH, GSH, GSH derivatized with Ellman's (GSH-Ell), and GSSG; (**c**) Optimization of HESI parameters on orbitrap mass spectrometer for the indicated metabolites using ZIC-pHILIC chromatography and standards. Graphs represent integrated areas of chromatographic peaks under changing parameters for capillary temperature or S-lens; (**d**) Limit of detection and linearity for individual redox molecules. Presented are the average values and standard deviation, where N – number of replicates; R^2 – goodness of fit; Sy.x - standard deviation of the residuals.

FIGURE 2
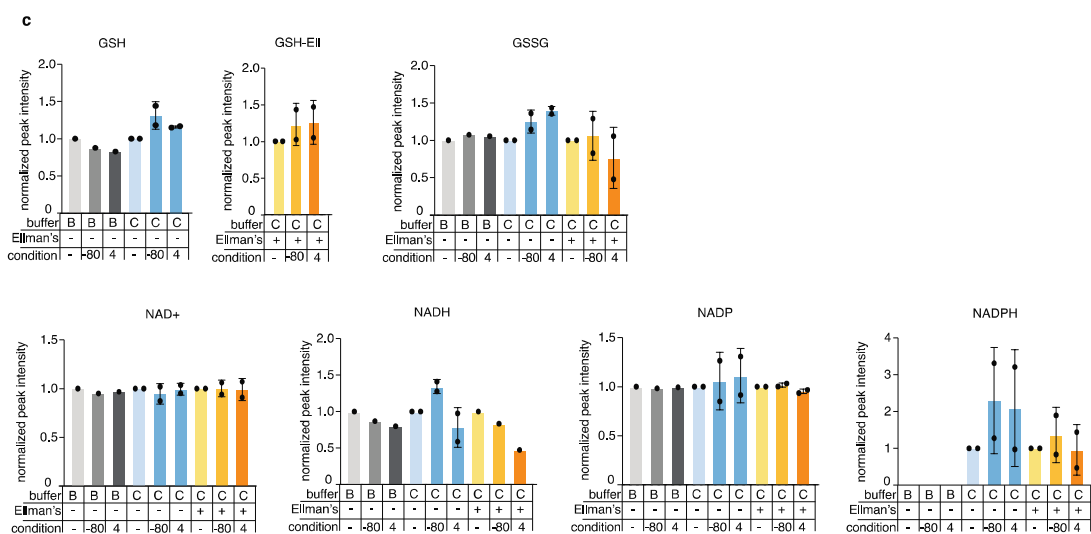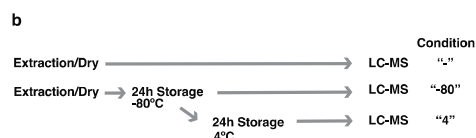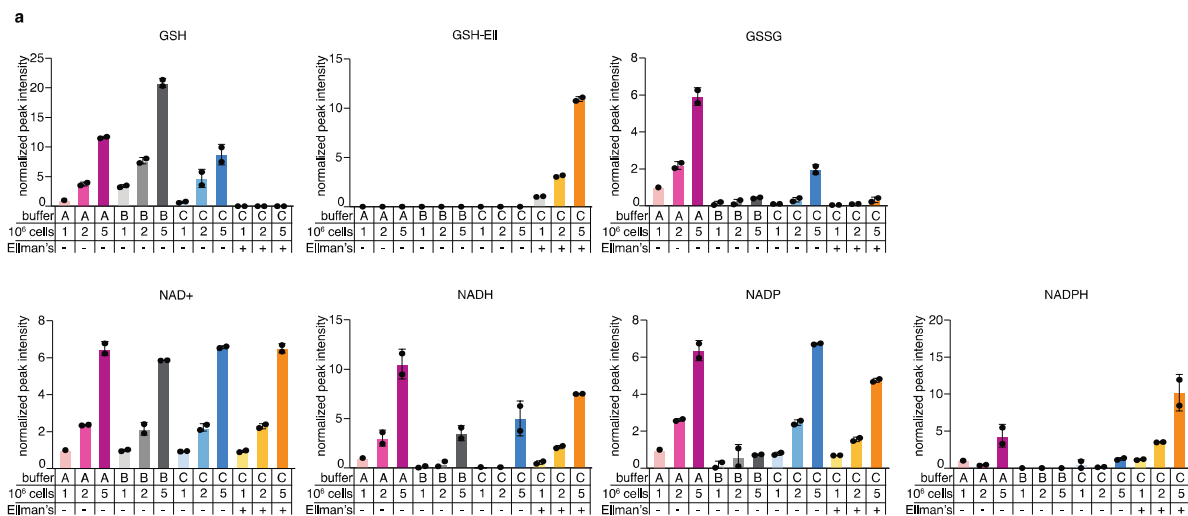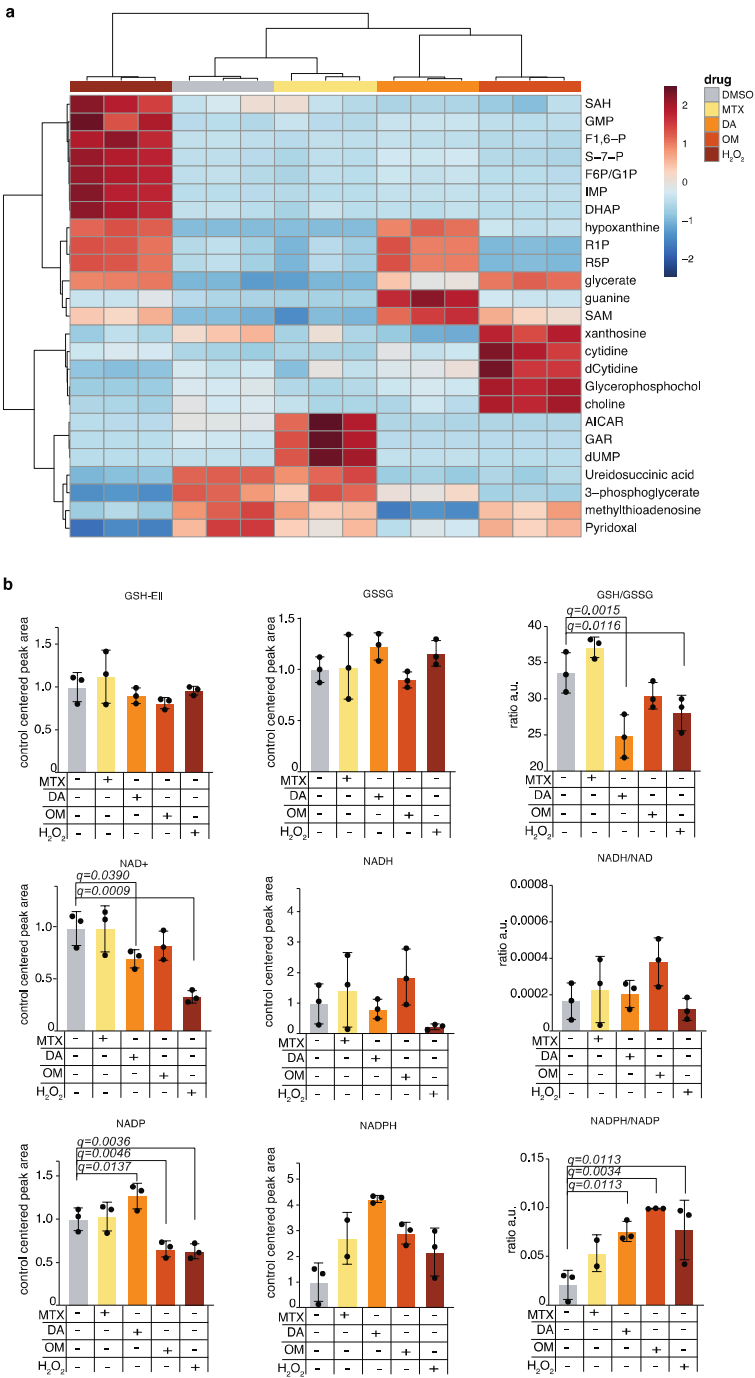
Figure 2. Optimization of redox metabolite detection in mammalian cells; (**a**) Comparison of metabolite detection in samples extracted from the mammalian cell line K562 using three extraction buffers (A, B, and C), with increasing number of cells (1, 2 or 5 million cells). Values were normalized to Buffer A/1 Million cells condition and present the average values and standard deviation of two experimental replicates, each with technical duplicates (except for buffer A, 1M condition, which was measured once with a technical duplicate; (**b**) A scheme of the metabolite stability tests performed of various storage conditions: One million K562 cells were extracted immediately upon harvest and either analyzed by LC-MS immediately (labeled "-"), or analyzed after they were stored for 24 hours at -80C° (labeled "-80"), or analyzed following reinjection that followed additional 24 hours incubation period at 4C° (labeled "4"); (**c**) Stability of redox metabolites in different storage conditions. Each storage condition was analyzed following extraction in the extraction buffers B and C. Values were normalized to the condition "-" that involved no long storage for each buffer. Presented are the average values and standard deviation of two independent experiments each with technical triplicates.

FIGURE 3

Figure 3. Application of the redox metabolite detection method for mammalian tissues; (**a** and **b**) Top 25 differentially detected metabolites between the three chromatographic methods in mouse liver (**a**) and kidney (**b**) presented in a heatmap for each organ. Each replicate is a tissue chunk from an independent mouse, extracted in buffer C+Ell and then split in three and run on the different chromatographies; (**c**) Global PCA analysis of polar metabolites detection in mouse liver samples extracted by three different buffers (B, C, C plus Ellman's) and detected by LC-MS using the ZIC-pHILIC column; Each replicate represents a liver chunk from an independent mouse, subdivided evenly between three tubes and extracted using the different buffers. This experiment was performed twice and a representative replicate is shown; (**d**) Top 25 differentially detected metabolites in mouse liver samples from (**c**); (**e**) Detection of redox metabolites from mouse liver, kidney, and CSF extracted in three different buffers (B, C, C plus Ellman's). This experiment was performed twice and a representative replicate is shown. Each dot represents a measurement from an independent mouse, mean and standard deviation are indicated; statistical significance was determined using Anova with correction for multiple comparisons by false discovery rate correction. Only significant q-values are indicated (except for GSH and GSH-Ell levels, which were excluded).

FIGURE 4

Figure 4. Application of the redox metabolite detection method for profiling redox state following pharmacologic perturbations of redox balance in cells; (**a**) K562 cells were treated with drugs that perturb the cellular redox balance and with H_2O_2, using the following doses for 4 hours: methotrexate: 5 μM; oligomycin: 80 μg/mL; H2O2: 1 mM; diamide: 0.5 mM; DMSO, which served as control: 0.6 μl per 1mL of cell culture media. The drugs used are diamide (DA), oligomycin (OM), and methotrexate (MTX). Global heatmap analysis of the top 25 differentially-changed polar metabolites is presented; (**b**) Detected levels of redox metabolites in the treated cells. Mean and standard deviation of three technical replicates are presented; statistical significance was determined using Anova with correction for multiple comparisons and false discovery rate. Only significant q-values are indicated.

3. Discussion

Here we report the optimization of an LC-MS detection method of redox metabolites suitable for parallel assessment of global metabolism from mammalian tissues. This method will be of interest for researchers from a wide variety of biological fields. We describe optimized detection of chemical standards of the redox metabolites, as well as optimized detection of the endogenous metabolites in mammalian cells and in mouse tissues – liver, kidney, and the CSF. Further, we measured the levels of redox metabolites in the cancer cell line K562 following pharmacological perturbation of the cellular redox state and demonstrate our ability to assess relevant metabolites in cells exposed to mild oxidative stress.

Our data suggest that optimal detection of redox metabolites can be achieved by extraction buffer C (Table 2) combined with Ellman's for GSH detection. This method does not compromise detection of majority of polar metabolites. Users may still wish to use the other buffers presented here depending on their interest in certain metabolites and according to the data presented here (Tables 1 and S3-4).

The comparison we present here between three different commercially available HILIC columns provides a comprehensive dataset that can help users decide on the optimal column for their needs (Figure S3a and Table S2). We recognize that our comparison is not exhaustive and that further conditions or set of small molecules can be found that showcase one column over another, yet the metabolites we have focused on here cover broadly major pathways of central carbon metabolism in mammalian cells. Finally, the ionization conditions optimized here will be broadly applicable to most Thermo model MS instruments, like orbitrap and triple quad mass spectrometers, which are widely used in the metabolomics community.

With the data we have presented here, we aim to facilitate successful study of the redox state of mammalian cells by applying metabolite profiling by LC-MS. Our method can be applied to address a wide variety of biological questions that involve oxidative stress or redox imbalance and can resolve a difficulty to directly measure redox metabolites in the context of global metabolic state.

4. Materials and Methods

Animal care, CSF and organ collection

All animal care and experimental procedures were approved by the Institutional Animal Care and Use Committees of Boston Children's Hospital. Mouse strain used was C57BL/6. Pure CSF samples were collected from the cisterna magna [39]. Blood samples were collected from the retromandibular vein. The samples were coagulated and centrifuged. Liver and kidney were collected and flash frozen. Tissue chunks were cut on a glass plate while kept chilled on top of dry ice.

Cell culture and treatments

K562 cells used in this manuscript were authenticated by short tandem repeat analysis and tested negative for mycoplasma. Cells were cultured in RPMI (Genesee Scientific) up to a density of 2 Million cells per ml. For redox chemical treatment experiments, cells were seeded at 1 Million cells per ml cell density in 6-well plates and drugs were added for 4h at the following concentrations: methotrexate: 5 μM; oligomycin: 80 μg/ml; H2O2: 1 mM; diamide: 0.5 mM; DMSO, which served as control: 0.6 μl per 1 mL of cell culture media (equivalent to volume used for oligomycin).

Sample preparation for LC-MS analysis of polar metabolites from tissues or cultured cells (with considerations for NADH and NADPH detection)

Metabolites were quenched as quickly as possible while working with the samples at low temperatures. Cells were handled at 4ºC or on dry ice, extraction buffer was pre-chilled at -20ºC. Samples were analyzed by LC-MS on the same day of extraction (if impractical, best alternative is to store <u>dried</u> samples at -80ºC). Unless indicated otherwise, 1 million cells or about 2 mg of tissue was extracted per condition and a minimum of three replicates per condition was used in each experiment. K562 cells that are non-adherent, were collected by brief centrifugation at 4ºC using a table-top centrifuge (4,500 rpm, 1.5 min) and washed briefly in 0.9% NaCl (high grade salt and LC-MS-grade water Fisher Scientific W6500 or Sigma Aldrich 1.15333). 300 µl of prechilled extraction buffer were added per sample. For tissues – chunks were crushed using a hand-held homogenizer (VWR 47747-370) with several pulses while keeping the samples on ice. 300 µl of prechilled extraction buffer was used per 2 mg of tissue.

Extraction buffer "A":

40:40:20 of acetonitrile:methanol:water, supplemented with 0.1M formic acid and isotopically-labeled internal standards (17 amino acids and reduced glutathione, Cambridge Isotope Laboratories, MSK-A2-1.2 and CNLM-6245-10).

Extraction buffer "B":

80% LC-MS-grade methanol, 20% 25 mM Ammonium Acetate and 2.5 mM Na-Ascorbate prepared in LC-MS water and supplemented with isotopically labeled internal standards (17 amino acids and isotopically labelled reduced glutathione, Cambridge Isotope Laboratories, MSK-A2-1.2 and CNLM-6245-10).

Extraction buffer "C" and "C + Ellman's":

Solution 1: 100% LC-MS Methanol

Solution 2: 25mM Ammonium Acetate and 2.5mM Na-Ascorbate in LC-MS water supplemented with isotopically labelled reduced glutathione and isotopically labeled internal standards (17 amino acids and reduced glutathione, Cambridge Isotope Laboratories, MSK-A2-1.2 and CNLM-6245-10).

Ellman's reagent (5,5'-Dithiobis(2-nitrobenzoic acid),D8130, Sigma Aldrich): 20 mM in "Solution 2". Final composition is 80% solution 1 and 20% solution 2.

Samples were vortexed briefly (10 sec) and sonicated for 3 min in a 4ºC water bath. Samples were then centrifuged for 10 min, 4ºC, at maximum speed on a benchtop centrifuge (Eppendorf) and the cleared supernatant was transferred to a new tube. Samples were dried using a nitrogen dryer while on ice, and special attention was given to minimize the time of drying and to not let samples idle in the dryer (Reacti-Vap™ Evaporator, Thermo Fisher Scientific, TS-18826) once the drying process was completed. Needles were continuously adjusted to the surface of the liquid as the samples evaporated to expedite the drying process. Samples were reconstituted in 30 µl LC-MS-grade water by brief sonication in a 4ºC water bath. Extracted metabolites were spun for 2 min at maximum speed on a bench-top centrifuge and cleared supernatant was transferred to LC-MS micro vials (National Scientific, C5000-45B). A small amount of each sample was pooled and serially diluted 3- and 10-fold to be used as quality controls throughout the run of each batch.

Sample preparation for LC-MS analysis of polar metabolites from CSF (with special considerations for NADH and NADPH detection)

CSF was collected by puncture of the cisterna magna with a glass capillary [39] and flash-frozen for further analysis. Per condition, 3 µl of precleared CSF were extracted by brief sonication in 200 µl of the indicated extraction buffers. After centrifugation for 10 min at maximum speed on a benchtop centrifuge (Eppendorf) the cleared supernatant was dried using a nitrogen dryer and reconstituted in 30 µl water by brief sonication. Extracted metabolites were spun again and cleared supernatant was transferred to LC-MS micro vials. A small amount of each sample was pooled and serially diluted 3- and 10-fold to be used as quality controls throughout the run of each batch.

Chromatographic conditions for LC-MS

ZIC-pHILIC chromatography: One ml of reconstituted sample was injected into a ZIC-pHILIC 150 × 2.1 mm (5 μm particle size) column (EMD Millipore) operated on a Vanquish™ Flex UHPLC Systems (Thermo Fisher Scientific, San Jose, CA). Chromatographic separation was achieved using the following conditions: buffer A was acetonitrile; buffer B was 20 mM ammonium carbonate, 0.1% ammonium hydroxide. Gradient conditions we used were: linear gradient from 20% to 80% B; 20–20.5 min: from 80% to 20% B; 20.5–28 min: hold at 20% B. The column oven and autosampler tray were held at 25 °C and 4 °C, respectively.

Accucore-HILIC chromatography: One ml of reconstituted sample was injected into a Thermo Fisher Scientific™ Accucore™ 150 Amide HILIC (150x3 mm, 2.6 mm particle size; Thermo Fisher Scientific) operated on a Vanquish™ Flex UHPLC Systems (Thermo Fisher Scientific, San Jose, CA). Chromatographic separation was achieved using the following conditions: buffer A was acetonitrile; buffer B was 20 mM ammonium carbonate, 0.1% ammonium hydroxide. Gradient conditions were: linear gradient from 20% to 80% B; 20–20.5 min: from 80% to 20% B; 20.5–28 min: hold at 20% B. The column oven and autosampler tray were held at 35 °C and 4 °C, respectively.

LUNA-NH2 chromatography: One ml of reconstituted sample was injected into a Luna® 3 μm NH2 100 Å, LC Column (150x2 mm, 3 μm particle size; Phenomenex, 00F-4377-B0) operated on a Vanquish™ Flex UHPLC Systems (Thermo Fisher Scientific, San Jose, CA). Chromatographic separation was achieved using the following conditions: buffer A was acetonitrile; buffer B was 5 mM ammonium acetate and 0.2% ammonium hydroxide. Gradient conditions were: 20 min linear gradient from 10% to 90% B; 20-25 min hold at 90% B; 25–26 min from 90% to 10% B; 26–34 min hold at 10% B. The column oven and autosampler tray were held at 30 °C and 4 °C, respectively

Orbitrap conditions for targeted analysis of polar metabolites

MS data acquisition was performed using a QExactive benchtop orbitrap mass spectrometer equipped with an Ion Max source and a HESI II probe (Thermo Fisher Scientific, San Jose, CA) and was performed in positive and negative ionization mode in a range of m/z= 70–1000, with the resolution set at 70,000, the AGC target at $1x10^6$, and the maximum injection time (Max IT) at 20 msec. For tSIM scans, the resolution was set at 70,000, the AGC target was $1x10^5$, and the max IT was 100 msec. For PRM scans, the resolution was set at 17,500, the AGC target was $1x10^5$, and the max IT was 20 msec. The following inclusion list and energies were used (Table 5):

Table 5. Inclusion list for PRM analysis of specified metabolites

Name	m/z	Polarity	NCE	RT range (min)
GSH-Ellman's	503.0552	negative	20, 40, 60, 80	8-12
GSH-13C2-15N-Ellman's	506.0580	negative	20, 40, 60, 80	8-12
GSH	308.0911	positive	20, 40, 60, 80	8-12
GSH-13C2-15N	309.0802	positive	20, 40, 60, 80	8-12
GSSG	613.1592	positive	20, 40, 60, 80	10-14
NADPH	746.0984	positive	20, 40, 60, 80	9-14
NADP	744.0827	positive	20, 40, 60, 80	8-13
NADH	666.1320	positive	20, 40, 60, 80	6-11
NAD+	664.1164	positive	20, 40, 60, 80	6-11

Data analysis and statistics

Relative quantitation of polar metabolites was performed with TraceFinder 4.1 (Thermo Fisher Scientific, Waltham, MA) using a 5 ppm mass tolerance and referencing an in-house library of chemical standards (Table 1 and Table S1). Pooled samples and fractional dilutions were prepared as quality controls and injected at the beginning and end of each run. In addition, pooled samples were interspersed throughout the run to control for technical drift in signal quality as well as to serve to access the coefficient of variability (CV) for each metabolite. Data normalizations were performed in two steps; 1. Integrated peak area signal from internal standards added to extraction buffers were mean-centered (for every standard, peak area was divided by the mean peak area of the set) and averaged across samples; samples were divided by the resulting factor, thus normalizing for any technical variability due to MS-signal fluctuation or pipetting and sample injection errors (usually withing 10% variability). 2. Normalization for biological material was based on detected metabolites as follows: CV values (based on pooled sample re-injections) and coefficient of determination (RSQ) (based on linear dilutions of pooled sample) were calculated per metabolite, metabolites with <30% CV and > 0.95 RSQ were mean-centered and averaged across samples. Samples were then divided by the resulting factor (biological normalizer) thus accounting for any global shift in metabolite amounts due to differences in biological material. When different cell numbers were used, normalization for biological material was performed as described above but the biological normalizer was divided by the fold change in cell number to preserve the global differences in total metabolite amounts.

For downstream MetaboAnalyst-based statistical or pathway analysis, the data were either Log transformed and Pareto scaled [40] or normalized to control conditions where indicated. All heatmap, PCA, or PLSDA analysis were performed using the MetaboAnalyst online platform. Individual one-way Anova and t-tests were performed in Prism software. Multiple comparisons correction and false discovery rate tests were based on the two-stage step-up method of Bejamini, Krieger and Yekuteili (as recommended within Prism software).

Data deposition information

All data generated as part of this method development is deposited at Metabolomics Workbench accession numbers will be added to the final version of this manuscript

The Committee for Animal Care at Boston Children's Hospital approved all animal procedures carried out in this study under protocol number 19-07-3936.

References

1.   Sies, H. and D.P. Jones, *Reactive oxygen species (ROS) as pleiotropic physiological signalling agents.* Nat Rev Mol Cell Biol, 2020. **21**(7): p. 363-383.

2.   Chandel, N.S., *Navigating Metabolism*. 2015: Cold Spring Harbor Laboratory Press.

3.   Auten, R.L. and J.M. Davis, *Oxygen toxicity and reactive oxygen species: the devil is in the details.* Pediatr Res, 2009. **66**(2): p. 121-7.

4.   Hayes, J.D., A.T. Dinkova-Kostova, and K.D. Tew, *Oxidative Stress in Cancer.* Cancer Cell, 2020. **38**(2): p. 167-197.

5.   Harris, I.S. and G.M. DeNicola, *The Complex Interplay between Antioxidants and ROS in Cancer.* Trends Cell Biol, 2020. **30**(6): p. 440-451.

6.   Kong, H. and N.S. Chandel, *Regulation of redox balance in cancer and T cells.* J Biol Chem, 2018. **293**(20): p. 7499-7507.

7.   Muri, J. and M. Kopf, *Redox regulation of immunometabolism.* Nat Rev Immunol, 2020.

8.   Lin, M.T. and M.F. Beal, *Mitochondrial dysfunction and oxidative stress in neurodegenerative diseases.* Nature, 2006. **443**(7113): p. 787-95.

9.   Xiao, H., et al., *A Quantitative Tissue-Specific Landscape of Protein Redox Regulation during Aging.* Cell, 2020. **180**(5): p. 968-983 e24.

10.   Woolley, J.F., J. Stanicka, and T.G. Cotter, *Recent advances in reactive oxygen species measurement in biological systems.* Trends Biochem Sci, 2013. **38**(11): p. 556-65.

11.   Murphy, M.P., et al., *Unraveling the biological roles of reactive oxygen species.* Cell Metab, 2011. **13**(4): p. 361-366.

12.   Griendling, K.K., et al., *Measurement of Reactive Oxygen Species, Reactive Nitrogen Species, and Redox-Dependent Signaling in the Cardiovascular System: A Scientific Statement From the American Heart Association.* Circ Res, 2016. **119**(5): p. e39-75.

13.   Dikalov, S.I., Y.F. Polienko, and I. Kirilyuk, *Electron Paramagnetic Resonance Measurements of Reactive Oxygen Species by Cyclic Hydroxylamine Spin Probes.* Antioxid Redox Signal, 2018. **28**(15): p. 1433-1443.

14.   Hou, C., et al., *Development of a Positron Emission Tomography Radiotracer for Imaging Elevated Levels of Superoxide in Neuroinflammation.* ACS Chem Neurosci, 2018. **9**(3): p. 578-586.

15.   Carroll, V., et al., *A boronate-caged [(1)(8)F]FLT probe for hydrogen peroxide detection using positron emission tomography.* J Am Chem Soc, 2014. **136**(42): p. 14742-5.

16.   Al-Karmi, S., et al., *Preparation of an (18) F-Labeled Hydrocyanine Dye as a Multimodal Probe for Reactive Oxygen Species.* Chemistry, 2017. **23**(2): p. 254-258.

17.   Oparka, M., et al., *Quantifying ROS levels using CM-H2DCFDA and HyPer.* Methods, 2016. **109**: p. 3-11.

18.   Eruslanov, E. and S. Kusmartsev, *Identification of ROS using oxidized DCFDA and flow-cytometry.* Methods Mol Biol, 2010. **594**: p. 57-72.

19.   Hanson, G.T., et al., *Investigating mitochondrial redox potential with redox-sensitive green fluorescent protein indicators.* J Biol Chem, 2004. **279**(13): p. 13044-53.

20.   Belousov, V.V., et al., *Genetically encoded fluorescent indicator for intracellular hydrogen peroxide.* Nat Methods, 2006. **3**(4): p. 281-6.

21.   Deidda, M., et al., *Metabolomic Approach to Redox and Nitrosative Reactions in Cardiovascular Diseases.* Front Physiol, 2018. **9**: p. 672.

22.   Wang, X., N.V. Shults, and Y.J. Suzuki, *Oxidative profiling of the failing right heart in rats with pulmonary hypertension.* PLoS One, 2017. **12**(5): p. e0176887.

23.   Liu, H., et al., *An Integrated LC-MS/MS Strategy for Quantifying the Oxidative-Redox Metabolome in Multiple Biological Samples.* Anal Chem, 2020. **92**(13): p. 8810-8818.

24.   Andrisic, L., et al., *Short overview on metabolomics approach to study pathophysiology of oxidative stress in cancer.* Redox Biol, 2018. **14**: p. 47-58.

25.   Chen, W.W., et al., *Absolute Quantification of Matrix Metabolites Reveals the Dynamics of Mitochondrial Metabolism.* Cell, 2016. **166**(5): p. 1324-1337.e11.

26.   Lee, C.C., et al., *The protein synthesis inhibitor blasticidin s enters mammalian cells via leucine-rich repeat-containing protein 8D.* J Biol Chem, 2014. **289**(24): p. 17124-31.

27.   Ellman, G.L., *Tissue sulfhydryl groups.* Arch Biochem Biophys, 1959. **82**(1): p. 70-7.

28.   Lu, W., et al., *Extraction and Quantitation of Nicotinamide Adenine Dinucleotide Redox Cofactors.* Antioxid Redox Signal, 2018. **28**(3): p. 167-179.

29.   Chen, L., et al., *An LC-MS chemical derivatization method for the measurement of five different one-carbon states of cellular tetrahydrofolate.* Anal Bioanal Chem, 2017. **409**(25): p. 5955-5964.

30.   Giustarini, D., et al., *Pitfalls in the analysis of the physiological antioxidant glutathione (GSH) and its disulfide (GSSG) in biological samples: An elephant in the room.* J Chromatogr B Analyt Technol Biomed Life Sci, 2016. **1019**: p. 21-8.

31.   Kim, Y.C., et al., *Thioredoxin-dependent redox regulation of the antioxidant responsive element (ARE) in electrophile response.* Oncogene, 2003. **22**(12): p. 1860-5.

32.   Salomon, A.R., et al., *Understanding and exploiting the mechanistic basis for selectivity of polyketide inhibitors of F(0)F(1)-ATPase.* Proc Natl Acad Sci U S A, 2000. **97**(26): p. 14766-71.

33.   Elango, T., et al., *Impact of methotrexate on oxidative stress and apoptosis markers in psoriatic patients.* Clin Exp Med, 2014. **14**(4): p. 431-7.

34.   Miyazono, Y., F. Gao, and T. Horie, *Oxidative stress contributes to methotrexate-induced small intestinal toxicity in rats.* Scand J Gastroenterol, 2004. **39**(11): p. 1119-27.

35.   Heidari, R., et al., *Mitochondrial dysfunction and oxidative stress are involved in the mechanism of methotrexate-induced renal injury and electrolytes imbalance.* Biomed Pharmacother, 2018. **107**: p. 834-840.

36.   Kozminski, P., et al., *Overview of Dual-Acting Drug Methotrexate in Different Neurological Diseases, Autoimmune Pathologies and Cancers.* Int J Mol Sci, 2020. **21**(10).

37.   Kuehne, A., et al., *Acute Activation of Oxidative Pentose Phosphate Pathway as First-Line Response to Oxidative Stress in Human Skin Cells.* Mol Cell, 2015. **59**(3): p. 359-71.

38.   Mullarky, E. and L.C. Cantley. *Diverting Glycolysis to Combat Oxidative Stress.* 2015. Tokyo: Springer Japan.

39.   Shipley, F.B., et al., *Tracking Calcium Dynamics and Immune Surveillance at the Choroid Plexus Blood-Cerebrospinal Fluid Interface.* Neuron, 2020. **108**(4): p. 623-639.e10.

40.   Pang, Z., et al., *MetaboAnalystR 3.0: Toward an Optimized Workflow for Global Metabolomics.* Metabolites, 2020. **10**(5).